JOURNAL OF AIRCRAFT
Vol. 44, No. 6, November–December 2007

Design of a Passively Reefed, Collapsible Drogue Parachute System

Stephen A. Whitmore*
Utah State University, Logan, Utah 84322-1400
and
Elsa J. Hennings†
Naval Air Warfare Center, China Lake, California 93555-6100

DOI: 10.2514/1.28437

A collapsible drogue parachute system developed for the X-37 approach and landing test vehicle is described. Originally, the approach and landing test vehicle test program called for a vehicle drop from a B-52 at 42,500-ft altitude. The approach and landing test vehicle relied on autonomous control for all phases of flight, including release, approach, and landing. If a software failure induced a control surface hardover during separation, the low vehicle weight and moderate subsonic lift-to-drag ratio made it possible for recontact with the B-52 after release. To eliminate recontact possibility, a drogue parachute system was installed. The drogue was deployed before the approach and landing test vehicle drop and was jettisoned after clean separation. The high altitude at drogue release allowed predominant winds to take the chute off the Edwards Air Force Base test range and into the flight corridors of major commercial airports. A mechanism to collapse to the drogue was required to keep the landing point within the test range. A simple passive-reefing mechanism that relied on a silicone band attached at the drogue skirt was developed. At high dynamic pressure the band stretched to the skirt diameter, causing negligible drag loss, but retracted and significantly reduced drag area after jettison. Test results and the design evolution are reported.

Nomenclature

C_D	=	drag coefficient
$C_D A_r$	=	reefed parachute drag area, ft^2
$C_D A_{\text{wake}}$	=	wake-adjusted parachute drag area, ft^2
$C_D A_0$	=	nominal parachute drag area, ft^2
D_b	=	effective base diameter of the wake-producing body, ft
D_p	=	inflated diameter of the parachute, ft
D_0	=	nominal or constructed parachute diameter, ft
$\mathrm{d}p$	=	pressure change rate, psf (mbar)
$\mathrm{d}Z$	=	altitude change, ft
$\mathrm{d}Z/\mathrm{d}t$	=	vertical velocity, ft/s
F_a	=	axial force, lbf
g_o	=	acceleration of gravity at sea level, 32.1738 ft/s
i	=	index
J	=	chute performance index
L	=	length of the test specimen, in.
L_r	=	reefing-line length, ft
L_{rate}	=	temperature lapse rate, °F/ft
Ls	=	suspension-line length, ft
L_T	=	distance from the aft end of the wake-producing body to the parachute skirt, ft
N	=	number of points in a data record
p	=	pressure, psf (mbar)
p_{ground}	=	barometric pressure at local ground level, psf (mbar)
$\bar{q}$	=	dynamic pressure, psf
R_g	=	gas constant for air, 53.355 ft · lbf/°R · lbm
T	=	temperature, °F (°C)
T_{ground}	=	ground temperature, °R (K)
T_r	=	reefing-line force, lbf
$T_{Z_{\text{drop}}}$	=	temperature at the parachute release altitude, °R (K)
W	=	parachute and tackle weight, lb
Z	=	geometric altitude, ft
Z_{drop}	=	geometric altitude at parachute release, ft
Z_{ground}	=	geometric altitude of the local ground level, ft
ΔL	=	elongation of the test sample, in.
δ	=	measurement uncertainty
θ	=	pitch coning angle, deg.
λ_g	=	geometric porosity, %
ρ	=	density, lbm/ft^3
σ	=	standard measurement error in drag area, ft^2
ψ	=	yaw coning angle, deg

Presented as Paper 873 at the 42nd AIAA Aerospace Sciences Meeting and Exhibit, Reno, NV, 5–8 January 2004; received 19 October 2006; revision received 6 July 2007; accepted for publication 7 July 2007.

*Assistant Professor, Mechanical and Aerospace Engineering Department, 4130 Old Main Hill, University Mail Code 4130. Associate Fellow AIAA.

†Recovery Systems Design Engineer, Weapons Division, Human Systems Department, Code 466100D. Member AIAA.

I. Introduction

THE X-37 vehicle was originally conceived as an integrated test bed to mature technologies critical to the advanced military space operations. The X-37 grew out of the X-40a program that teamed the U.S. Air Force with NASA and the Boeing Company in a cooperative agreement to develop a small, highly maneuverable, reusable spacecraft known as the space maneuvering vehicle. A comprehensive series of X-40a flight tests was concluded at Edwards Air Force Base, California in the spring of 2001. The X-37 vehicle is a larger-scale version of the X-40A, with some outer mold lines modified to provide better hypersonic and supersonic performance and flying qualities. As the program was originally proposed, Boeing's Phantom Works division in Palmdale, California would build two X-37 airframes. Vehicle 1, dubbed the approach and landing test vehicle (ALTV), was designed for a series of atmospheric flight tests to evaluate the subsonic flight characteristics and to validate the guidance, navigation, and control systems and algorithms used for landing the spacecraft. Vehicle 2, dubbed the orbital vehicle, was proposed to be "spaceworthy" and would demonstrate all mission phases, including, launch, orbital deployment, orbital operations, and autonomous entry, descent, and landing.

NASA's original plan for testing of the X-37 ALTV called for carrying the vehicle aloft over the Edwards Air Force Base test range on a B-52 H-model aircraft and releasing it at Mach 0.7 and an

altitude of 42,500-ft mean sea level (MSL) [1]. In 2003, NASA determined that the X-37 ALTV did not meet the goals of the Vision for Space Exploration and, as a result, transferred the program to the Defense Advanced Research Projects Agency (DARPA). As the responsible test organization for the X-37 program, DARPA decided to use the Scaled Composites (Mojave, California) White Knight® instead of the B-52 for the carrier aircraft as a cost-saving measure. The ALT performed its first free flight in April 2006. During this flight, the vehicle successfully performed the separation, free flight, and approach and landing maneuvers. After landing, however, the vehicle encountered difficulties with its braking system and rolled off the end of a runway [2]. Some damage to the nose gear was sustained. After repairs to the vehicle, the X-37 ALTV program was concluded in 2006 with two additional successful test flights.

Although technically still alive, the future of the orbital program is unclear at this time. On 17 November 2006, Space.com reported that "The U.S. Air Force announced today that it is developing an orbital test vehicle (OTV), based on the design of a NASA X-37 craft. It is to be designated as the X-37B orbital test vehicle" [3]. The first flight for this classified program was reported as scheduled for fiscal year 2008, launching on an Atlas V from Cape Canaveral. The new OTV effort dovetails off of industry and government investments by the U.S. Air Force, NASA, and DARPA. The OTV effort will be led by the U.S. Air Force Rapid Capabilities Office and includes partnerships with NASA and the U.S. Air Force Research Laboratory. Boeing is the prime contractor for the OTV program. According to a statement from the Secretary of the Air Force, the OTV program will focus on "risk reduction, experimentation, and operational concept development for reusable space vehicle technologies, in support of long term developmental space objectives."

This paper details the development of a unique collapsible drogue parachute system that was originally developed for the NASA program in which the X-37 was to be released from the B-52 carrier aircraft. While performing hazard analyses of the B-52/X-37 separation event, the X-37 test team identified several potential software failures that resulted in hardover of one or more aerodynamic control surfaces. This scenario resulted in a potential for recontact of the X-37 with the B-52 after release. To eliminate the possibility of recontact, several mitigation strategies were investigated. The strategy finally selected involved deployment of a drogue parachute from the ALTV before release from the B-52. This parachute lowered the effective lift-to-drag ratio of the system to where recontact was impossible. A parachute with approximately 3300 lb of drag force was required to eliminate recontact for 99.9% of the failure scenarios. The drogue parachute was then to be jettisoned from the ALTV approximately 2.5 s after launch. After jettison from the X-37, the drogue chute, swivel, and attachments fall to the ground. Because of the high altitude at which the drogue is jettisoned, the predominant wind direction, and the close proximity of an air corridor of a major commercial airport, the drogue was required to collapse or significantly reduce its drag area after jettison to minimize its drift potential. A 50% reduction in the postjettison drag area of the drogue chute was required to keep the chute on the Edwards Air Force Base test range.

II. Parachute Collapse Mechanism

During the ALTV flight tests, the B-52 had capability for a maximum of three 15-min test runs before returning to base. Because the drogue chute is deployed before the ALTV release, if all three test runs were necessary before the ALTV was dropped, the parachute could potentially be deployed for up to 45 min. This long deployment time necessitated the use of a swivel on the drogue to prevent premature collapse or entanglement before the ALTV drop. Several methods, such as releasing a riser or lines, could be used to collapse the parachute after the jettison, but when a swivel is present in the system and located at the end of a long riser, this method becomes very complex to implement. Additionally, if the riser or lines released prematurely, there would be insufficient drag to prevent ALTV recontact. The method chosen for this system must be designed such that if it failed it would not impact the prerelease drag area of the parachute.

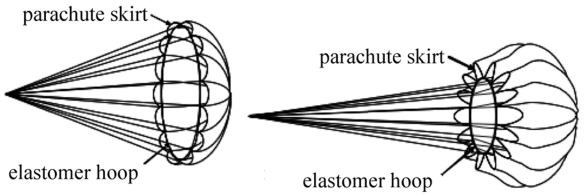

a) Fully open parachute b) Collapsed parachute

Fig. 1 Illustration of passive collapse concept.

Based on these requirements, the proposed design was an elastomer hoop attached at the skirt of the parachute. The elastomer would stretch to the projected diameter of the parachute while attached to the ALTV due to aerodynamic loading (see Fig. 1a) and then retract to its original length when the drogue jettisoned (see Fig. 1b). In this manner, if the elastomer failed before the ALTV jettison from the B-52, the parachute's drag would not be affected and would still allow a safe separation.

The first design hurdle for this system was to find an elastomer that would remain elastic at the low temperatures encountered at the drop altitude of 42,500-ft MSL. Based on historical upper-air-temperature data at Edwards Air Force Base [4], −90°F were chosen as the worst-case design temperature. The major potential roadblock to implementing this system is the inability of the elastic line to effectively operate at the extremely low temperatures. This very-low-temperature requirement quickly narrowed down the field of prospective products, and a suitable polymer, phenyl-methyl, dimethyl silicone, was identified. This product is available under the commercial brand name of Dow Corning Silastic® 3-6121 and is typically used as a low-temperature encapsulant for space-qualified electronics. Because the ATLV application of this material was atypical and the stress–strain properties not well-known, significant testing at both ambient and cold temperatures was necessary.

III. Initial Elastomer Testing and Evaluation

It was first necessary to ensure that the elastomer is functional at the anticipated worst-case temperature of −90°F and, once demonstrated as viable, to determine the stress–strain relationships. It was also necessary to determine the force that the full-open drogue parachute applies to the elastomer reefing band design, as well as the force necessary to collapse the parachute following jettison. These data allow the cross-sectional diameter of the reefing line, as well as the hoop diameter, to be properly sized. In addition, it was necessary to verify that the elastomer is capable of elongating at the chute opening rate without becoming plastic or structurally failing. Finally, the deployed reefing system was required to withstand up to 45 min under a full drag load at −90°F and still be elastic and pliable.

Test samples were fabricated at the U.S. Naval Air Warfare Center (NAWC) by mixing the two-part elastomer, degassing to remove seeds in the mixture, and pumping the still-wet polymer material into plastic tubing molds, in which it was cured at room temperature. When the elastomer cured, the tubing was scored down the entire length and peeled from the molded line. Cylindrical elastomer samples were fabricated for the initial testing. Length extension (strain) was measured by attaching a string-extensometer to the sample. The results from the initial testing were promising. Representative test results are shown in Fig. 2 for a 0.5-in-cross-sectional-diam line. The elastomer was fully elastic at 100% elongation, and the properties of the material at −65°F were nearly identical to the properties at ambient temperature. At −90°F, a small amount of hysteresis was present as the load was dropped, but disappeared when the sample warmed to ambient. Results from 45-min-duration tests, performed at 100% elongation ($\Delta L/L = 1.0$) and −90°F, showed that when warmed slightly the material retracted completely, with no hysteresis. Several samples with cross-sectional diameters varying from 0.1 to 1.0 in. were fabricated and tested to determine their tensile force at 100% elongation. Figure 3 plots the

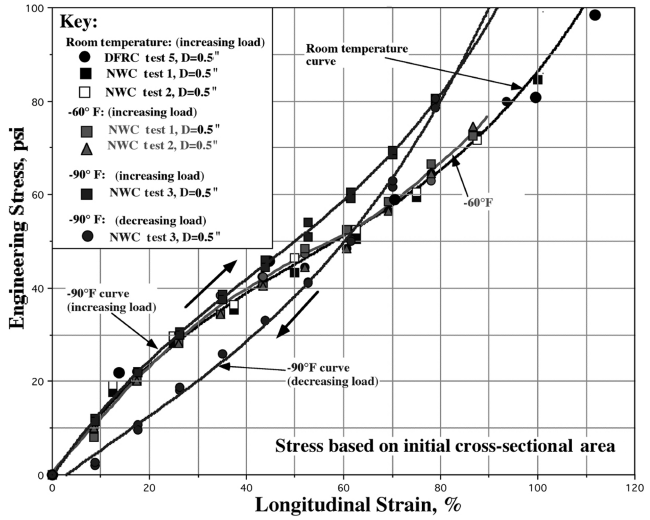

Fig. 2 Stress–strain curves for a 0.5-in.-cross-sectional-diam Dow Corning Sylastic 3-6121 test sample at room temperature, −60°F and −90°F.

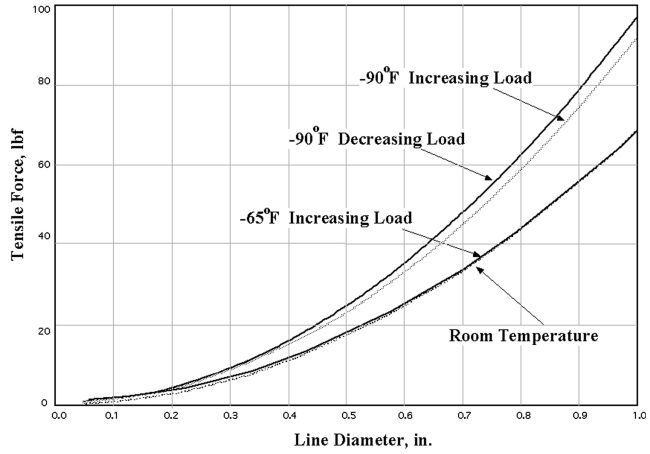

Fig. 3 Effect of line cross-sectional diameter on tensile force required for 100% elongation.

tensile force at 100% elongation as a function of the line cross-sectional diameter. Beyond the 0.5-in. cross-sectional diameter, the 100% elongation force rises dramatically.

The final laboratory test consisted of two dynamic onset tests at −90°F. In these dynamic loading tests, the elastomer line was stretched to 100% elongation in 0.153 s. This time was the calculated fill time of the unreefed drogue parachute at the deployment conditions. This test was performed by attaching a plate to the elastomer line with a Kevlar line routed through a hole in the bottom of the cold chamber. A 14-lb stack of weights was raised 7 in. above the plate and dropped onto the plate, generating the force required to extend the elastomer 100% in 0.153 s (the plate hitting the floor limited the extension to 100%). Figure 4a shows the experimental apparatus used for the shock load tests, and Fig. 4b shows the two test time histories. As shown, the elastomer successfully stretched to 100% elongation in approximately 0.15 s for both tests. Posttest inspection showed no visible damage to the specimen, and the differences between the trials is negligible.

IV. Reefing-Line Cross-Sectional-Diameter Sizing

Once the initial qualification tests determined that the material functioned adequately for the passive-reefing-line purpose, it became necessary to determine the reefing-line sizes necessary to achieve the stated requirements. To determine the cross-sectional diameter of line required for the reefing system, it was necessary to calculate the force that the parachute exerts on the line when it is fully open, which gives us a maximum line-retraction force and hence maximum cross-sectional diameter. It was also necessary to calculate the force exerted by the parachute after it was released from the ALTV, which gives a minimum required retraction force, hence a minimum line cross-sectional diameter. To determine these forces, data from Wolf and Croll [5] were used. In this paper, the ratio of the reefing-line force to the axial force was correlated for various reefing ratios and geometric chute porosities. Figure 5 shows the correlation data for a reefed ribbon parachute with 25% geometric porosity and suspension-line length to chute diameter ratios of 1.0, 1.5, and 2.0. Figure 5a shows the effect of the reefing-line ratio (the ratio of reefing-line length to constructed chute circumference) on the effective drag area ratios. Figure 5b shows the ratio of reefing-line force to axial force acting on the parachute. Using the data from Fig. 4 for a 20% conical drogue parachute with a porosity of 25% and a

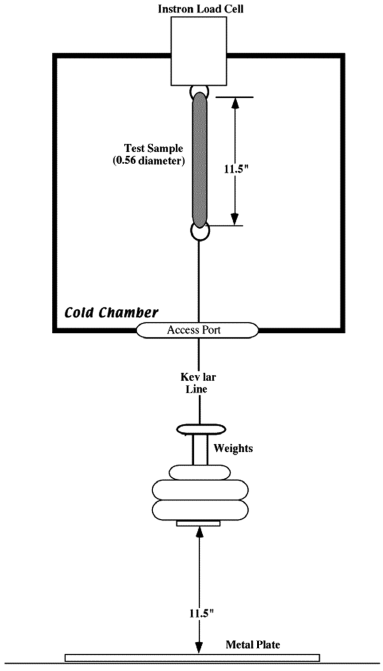

a) Test apparatus

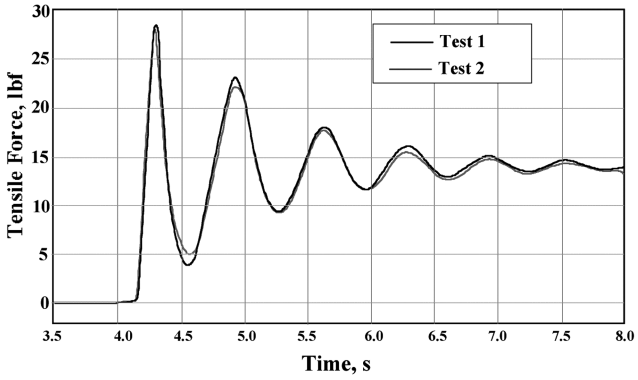

b) Load plot, -90°F, preloaded test specimen

Fig. 4 Apparatus schematic and test time histories for dynamic loading tests.

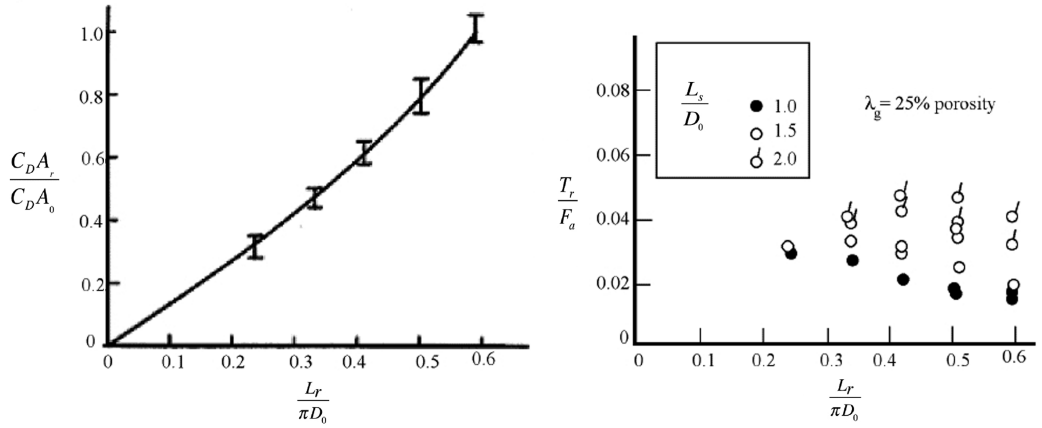

a) Reefed drag area ratio **b) Reefing line force ratio**

Fig. 5 Reefed drag area and reefing-line force ratio as function of reefing-line ratio.

suspension-line-to-diameter ratio of 1.0; for a full-open drag force of approximately 3300 lb, the full-open force in the reefing line was calculated to be a minimum of 66 lb. Assuming a canopy weight (and thus drag force) of 12 lb and reefing-line ratio of 0.35 (reefing-line ratio required for a 50% reduction in drag area), the force on the line after release of the drogue (at terminal velocity) is calculated to be approximately 0.4 lb. Therefore, the line must be capable of exerting more than 0.4 lbf but less than 66 lbf to function as desired.

Examination of the tensile force data presented in Fig. 3 shows that at 100% elongation, a 0.5-in-cross-sectional-diam line exerted a tensile force slightly over 25 lb at −90°F. This amount of force would insure that the chute would fully inflate at the nominal load of the parachute. Examination of the stress–strain data of Fig. 3 shows that at 10% elongation, the tensile load exerted by a 0.5-in. reefing line is approximately 2.4 lb, more then sufficient force to overcome the aerodynamic forces at terminal velocity when the chute has been jettisoned. Based on these calculations, it was decided that an elastomer reefing line with a 0.5-in. cross-sectional diameter would offer sufficient margin at both high (prerelease) and low (postrelease) flight loads to accomplish the requirements outlined earlier.

V. Drop-Tower Testing

Now that the material was proven to function adequately for the passive-reefing purposes and the proper cross-sectional line diameter and hoop circumference was determined, the reefing line was integrated into a parachute system and its low-speed performance was evaluated by drop-tower testing. These tests were conducted at the NAWC Echo Range drop towers. A picture of the drop towers is shown in Fig. 6.

Fig. 6 The 350-ft Echo Range drop towers.

The goal of these tests was to evaluate the effects of the reefing system on three candidate parachutes. For these tests, the 0.5-in.-diam (cross section) elastomer hoop with a circumference of 9.9 ft and a 100% elongation (19.8-ft circumference) Kevlar overinflation control line were attached to the skirt of the three parachutes. The design was intended to produce approximately 50% reduction in the nominal chute drag area. The overinflation line was used to insure that the elastomer line was not inflated beyond its elastic limit. The three parachutes tested were 1): a 9.3-ft-reference-diam, 24%-geometric-porosity ribbon parachute, 2) a 9.3-ft-reference-diam, 28%-geometric-porosity ribbon parachute, and 3) an 8.5-ft-reference-diam, 24% geometric-porosity ring-slot parachute. The parachute system weights were approximately 12.0 lb. This weight is atypical for chutes this size, with the built-in robustness in anticipation of the potential 45-min flight duration required for the ALTV flights. The local ground altitude at the Echo test site is 2315.1 ft above mean sea level (MSL).

Figure 7 shows a schematic of the test apparatus. A pressure sensor and a data recorder were attached to each parachute, and these were used to record pressure–time histories as the chute released and fell to the ground. A meteorological data package attached to the lifting cable (tethersonde) was used to telemeter pre- and postdrop temperatures, pressures, and wind speeds at the drop altitude to the ground. Following the chute drop and landing, the tethersonde was lowered to record ground temperature, pressure, and wind speed.

The hydrostatic equation [6] was used to transform the sensed pressure–time history data in to geometric altitude estimates. This

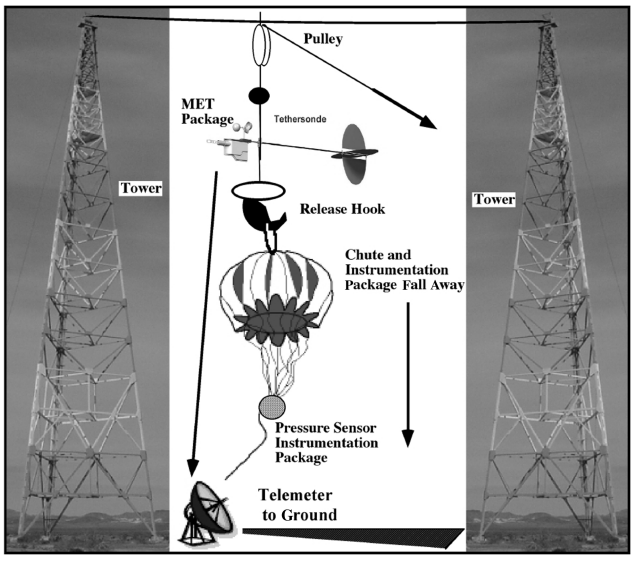

Fig. 7 Schematic of apparatus for Echo Range drop tests.

calculation is

$$\frac{\mathrm{d}p}{p} = -\frac{g_0}{R_g}\frac{\mathrm{d}Z}{T} \tag{1}$$

Temperature was related to altitude using a linear lapse rate equation:

$$\begin{aligned} T(Z) &= T_{\text{ground}} + L_{\text{rate}}[Z - Z_{\text{ground}}] \\ &= T_{\text{ground}} + \frac{T_{Z_{\text{drop}}} - T_{\text{ground}}}{[Z_{\text{drop}} - Z_{\text{ground}}]}[Z - Z_{\text{ground}}] \end{aligned} \tag{2}$$

The length of hoist cable required to lift the package to the drop altitude measured the drop altitude. As mentioned previously, the drop and surface pressures were obtained using the tethersonde package. Equation (2) is substituted into Eq. (1) and integrated to give

$$\begin{aligned} \ell_n\left[\frac{p(Z)}{p_{\text{ground}}}\right] &= -\frac{g_0}{R_g}\int_{Z_{\text{ground}}}^{Z}\left[\frac{\mathrm{d}Z}{T_{\text{ground}} + L_{\text{rate}}[Z - Z_{\text{ground}}]}\right] \\ &= -\frac{g_0}{R_g}\ell_n\left[1 + \frac{L_{\text{rate}}}{T_{\text{ground}}}(Z - Z_{\text{ground}})\right] \end{aligned} \tag{3}$$

Solving for Z gives

$$Z = Z_{\text{ground}} + \frac{T_{\text{ground}}}{L_{\text{rate}}}\left\{\left[\frac{p_{\text{ground}}}{p(Z)}\right]^{\frac{L_{\text{rate}}R_g}{g_0}} - 1\right\} \tag{4}$$

Given the recorded pressure–time history, Eq. (4) is used to calculate the geometric altitude–time history. The altitude–time history is numerically differentiated to give the vertical velocity of the parachute.

Each parachute was lifted to approximately 250 ft above ground level and released. A total of nine tests were conducted, two for each parachute in the normal canopy-above-payload configuration and one in an inverted configuration to evaluate the parachute's ability to right itself. Figures 8 and 9 show a typical set of results for the first drop of the 24%-porosity ribbon parachute with the elastomer reefing line. Figures 8a and 8b show the tethersonde data (attached to the chute hoist) used to obtain pre- and postdrop zeros for temperature and pressure. These data were also used to calculate the temperature lapse rate. The measured distance from the drop point to the ground was 246.1 ft. The data indicate that a small temperature rise occurred during the process of hoisting the parachute, preparing for drop, and then dropping. When this temperature rise is taken into account, the approximate temperature lapse rate was calculated as -0.004°C/ft (-13.3°C/km). Using the calculated lapse rate, the sensed pressure data from the onboard parachute sensor were used to calculate the differential altitude–time history. These data are shown in Figs. 8c and 8d.

The altitude position data shown in Fig. 8 are differentiated to calculate the vertical velocity of the parachute. Using the sensed pressure data, the calculated lapse rate, and the general gas law, the density and dynamic pressure profiles are also calculated. The vertical velocity and dynamic pressure plots are presented in Figs. 9a and 9b.

$$\rho(Z) = \frac{p(Z)}{R_g T(Z)} = \frac{p(Z)}{R_g(T_{\text{ground}} + L_{\text{rate}}[Z - Z_{\text{ground}}])} \tag{5}$$

$$\bar{q} = \frac{1}{2}\rho(Z)\left(\frac{\mathrm{d}Z}{\mathrm{d}t}\right)^2 \tag{6}$$

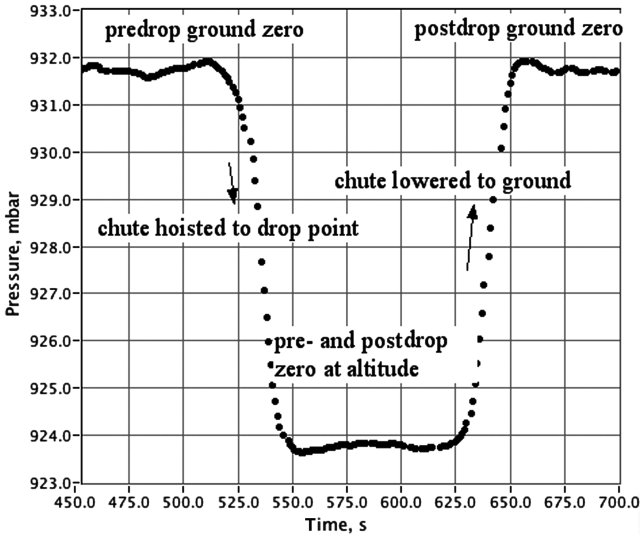

a) Sensed ambient pressure

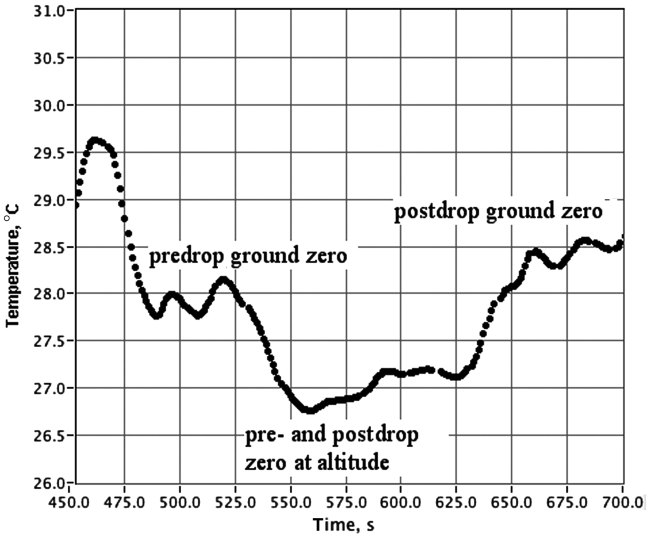

b) Sensed ambient temperature

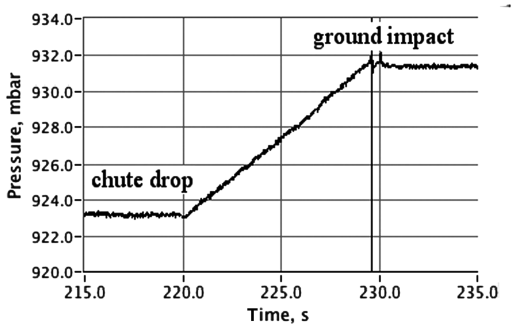

c) Onboard pressure time history during drop

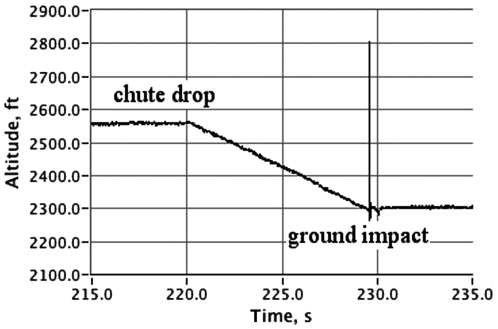

d) Calculated drop altitude time history

Fig. 8 Example drop time history data, 24% ribbon chute, test 1.

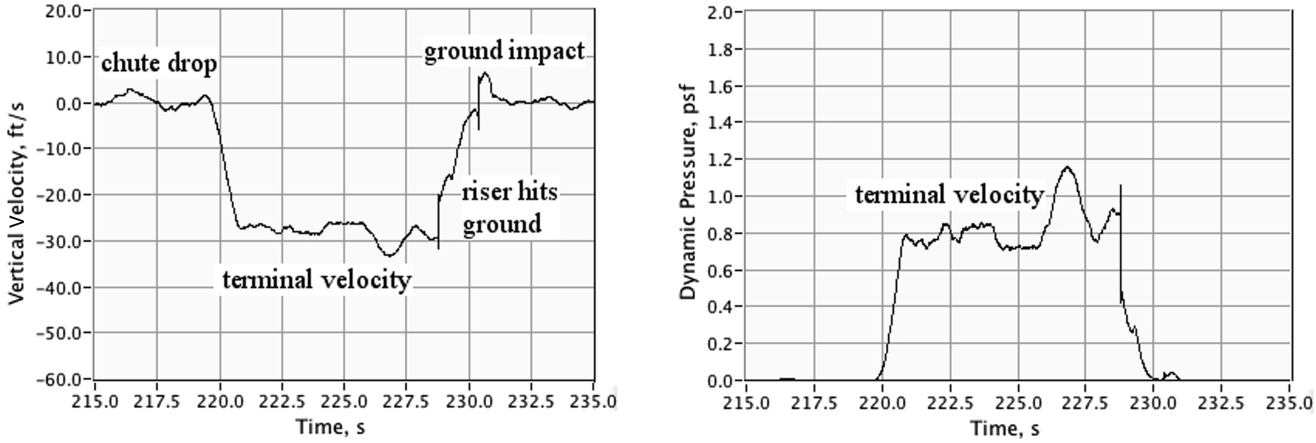

a) Calculated vertical velocity **b) Calculated dynamic pressure**

Fig. 9 Calculated vertical velocity and dynamic pressure, 24% ribbon chute, test 1.

In the example presented in Fig. 9, the chute reaches terminal velocity at approximately −29 ft/s, and the dynamic pressure at terminal velocity is approximately 0.8 psf. The drag area of the parachute is calculated by equating the drag force at the terminal velocity to the weight of the parachute. For example, if the chute weighed 12.61 lb, and the terminal dynamic pressure was 0.79 psf, the calculated drag area is

$$C_D A = \frac{Wt}{\bar{q}} = \frac{12.61}{0.79} = 15.96 \text{ ft}^2 \tag{7}$$

Similar results were obtained for each of the three parachutes. Table 1 summarizes the results of the drop tests for the three parachute configurations. Averaging the dynamic pressure over the terminal-velocity phase of flight and dividing that number into the measured parachute weight calculated the numbers presented in Table 1. The terminal-velocity flight phase was selected by inspection of the velocity–time history plots. Table 1 also lists standard error in the calculated drag areas and area ratios, based on the standard deviation in the calculated dynamic pressure over the terminal-velocity flight phase. Assumed accuracy in the weight measurements was based on the resolution of the scale used to weigh the parachute and tackle ∼0.01 lb. Equation (8) shows the process used to calculate the uncertainty of the drag area measurements.

$$\sigma[C_D A] = \sqrt{\left(\frac{\delta W}{\bar{q}}\right)^2 + \left(\frac{W}{\bar{q}}\delta\bar{q}\right)^2} \tag{8}$$

This preliminary drop-testing showed that the elastomer performed as expected at low speeds, reducing the drag area of each parachute to approximately 50% of the designed full-open drag area. All inverted canopies were able to right themselves, typically in about 2–3 s. The elastomer reefing system appeared to be fully function at low-speed conditions.

VI. High-Speed Ground Testing

For the next phase of testing, it was necessary to measure the performance of the drogue parachute candidates and the passive-reefing system at dynamic pressure close to the actual flight conditions. As mentioned in the Introduction, 3300 lbf of drag force was required to insure a safe separation event. At the launch dynamic pressure (∼120 psf), this drag force required approximately 27.5 ft^2 of drag area. Because the chute was to be deployed behind the X-37, the effects of the vehicle wake needed to be taken into account [7]. A drag loss of 6% was allowed for the X-37 wake, giving a required freestream drag of 29.15 ft^2. The plan was to characterize the fully inflated drag area of the chute systems (with the elastomer reefing system attached) and subsequently adjust the circumference of the overinflation hard line (using the relationship plotted in Fig. 5a) to give the desired drag area of 29.15 ft^2. In addition to drag area requirement, other X-37 requirements for the chute system were 1) the ability to properly inflate at flight dynamic pressure level, 2) coning angles in pitch and yaw axes less than 5 deg, 3) drag area ∼29.15 ft^2, 4) distinct chute coning frequencies greater than 1.5 Hz, 5) the ability to survive endurance testing for 45 min at flight dynamic pressure, and 6) the ability to collapse to 50% of full-open drag area after release from the X-37.

The High-Velocity Airflow System (HIVAS) facility, located at the NAWC in China Lake, was used to perform the high-speed tests. The bypass airflow from four TF-33 P11 engines ducted to a single nozzle provides the HIVAS flow. At maximum throttle setting for the engines (110%), the core airflow velocity is greater than 300 kt. At the altitude of the HIVAS facility (2600 ft), this flow velocity produced a core dynamic pressure of approximately 285 psf, considerably more than required to match the ALTV drop flight condition. The goals of the HIVAS tests were to produce two chute designs that satisfy the preceding criteria and to bring these designs forward for flight-testing. Results of the flight tests ultimately would determine the selection of a single parachute design for the X-37 free-flight tests.

A. HIVAS Phase I

During the first phase of high-speed testing, a model of the X-37 forebody was positioned in the flowfield to model the effects of the X-37 wake. All three parachutes had the elastomer hoop attached to the skirt, as installed for the drop-tower tests. A total of 21 runs were

Table 1 Summary of Echo Range drop-test results

Test, chute	Weight, lb	Dynamic pressure at terminal velocity, psf	Calculated $C_D A$, ft^2	Nominal drag area (design, ft^2)	Measured drop time, s	Mean $C_D A$ ratio
Drop 1, 24% ribbon	12.61	0.790 ± 0.021	15.96 ± 0.42	31.5	9.31	0.507 ± 0.013
Drop 2, 24% ribbon	12.61	0.804 ± 0.022	15.69 ± 0.43	31.5	9.38	0.498 ± 0.014
Drop 1, ring slot	12.13	0.608 ± 0.024	19.95 ± 0.79	34.0	10.07	0.587 ± 0.023
Drop 2, ring slot	12.13	0.633 ± 0.019	19.15 ± 0.58	34.0	9.83	0.560 ± 0.017
Drop 1, 28% ribbon	12.21	0.792 ± 0.020	15.41 ± 0.39	31.5	9.40	0.489 ± 0.012
Drop 2, 28% ribbon	12.21	0.786 ± 0.023	15.54 ± 0.45	31.5	9.38	0.493 ± 0.014

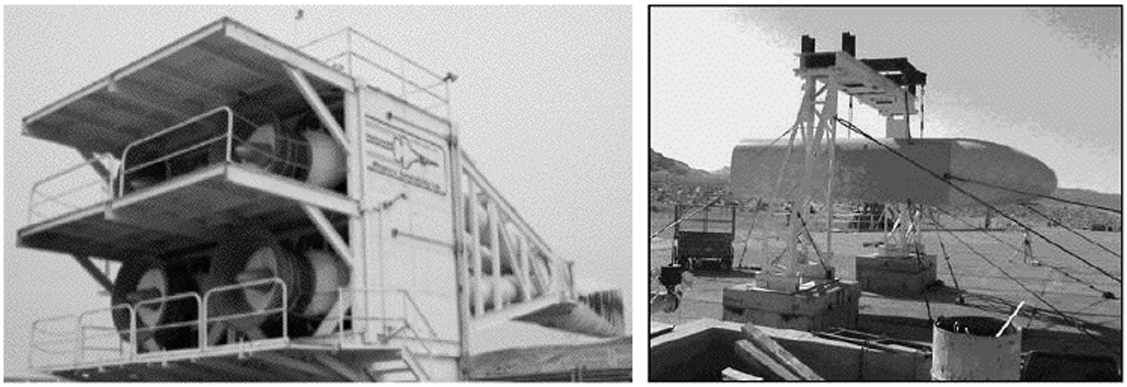

Fig. 10 X-37 forebody model as installed at the HIVAS facility.

performed during the initial testing phase with the X-37 drogue chute test fixture in place. The majority of the testing (17 runs) was performed with a riser length that positioned the parachute skirt 35.5 ft aft of the model base. Each of the three candidate chutes was also tested at the longest length of 48 ft (three runs), with only the ring-slot chute tested at the shortest distance of 25 ft (one run). Once testing began, it quickly became obvious that the achieved dynamic pressure levels were far below those anticipated. Subsequent pressure surveys with the X-37 forebody in the flowfield indicated that the achieved dynamic pressure levels in the vicinity of the parachute skirt were only 25–40% of the required flight level, even with all four engines operating at 100% thrust. Because the full flight load dynamic pressures (approximately 120 psf) could not be achieved with the X-37 forebody in the flow, the decision was made to remove the forebody model for the remainder of the tests. The one major quantitative result of the phase-I tests was the observation that the performance of the 28%-porosity ribbon-parachute performance was unacceptable. This parachute had significant inflation problems that initially were assumed to arise from the elastomer hoop. When the elastomer was removed, the chute still would not inflate properly. Because of the poor inflation characteristics, the 28% ribbon parachute was abandoned for further HIVAS testing. Figure 10 shows the HIVAS facility and the drogue chute test fixture as installed in the facility.

B. HIVAS Phase II

The second phase of high-speed testing was performed with the X-37 forebody removed from the flowfield and the parachute attached downstream of the nozzle. Full flight dynamic pressures were easily achieved with the X-37 forebody removed. The primary instrumentation fixture for this phase of testing was a custom-designed load balance that allowed the chute to be positioned in the center of the flowfield. A custom-designed pole-mounted force balance allowed the axial load of the parachutes to be measured in real time. The balance was designed to pivot in the pitch and yaw axes and allowed the parachute aerodynamic forces to always remain directly along the longitudinal axis of a load cell attached to the riser. This arrangement allowed the load cell to always sense the total aerodynamic load acting on the parachute. Roll-induced forces on the chute riser were relieved by a swivel attachment at the downstream end of the riser. Figure 11 depicts the load balance. To sense coning dynamics (amplitude and frequency), additional sensors were mounted on the swivel arm of the balance. These sensors include a three-axis rate gyro package, a three-axis linear accelerometer, and pitch- and yaw-angle control position transducers. The dynamic sensor information was blended using a Kalman filter [8] to reduce noise, vibration contamination, and add response fidelity. The filter output time tagged estimates of the chute loads in three axes and of the angular position and velocity in the pitch and yaw axes.

Phase I testing at HIVAS had shown that the flowfield is nonuniform across any given cross section and also varies as a function of distance aft from the HIVAS nozzle exit plane. This flowfield nonuniformity means that the drogue chute experiences a different *effective* dynamic pressure, depending on its position within the flowfield. These variations must be accounted for when calculating the chute drag areas from the raw force measurements. To capture this measurement, a pitot tube mounted on the parachute riser line was designed for the HIVAS tests. The pressure signal from the pitot tube was transmitted to a pressure transducer mounted on the instrumentation pallet via a length of plastic tubing sewn to a parachute riser. Ambient pressure was obtained by routing a length of tubing from the instrumentation pallet to a location well outside of the HIVAS flowfield. Pneumatic lags on the pitot measurement were measured to be less than 0.07 s and were considered to be acceptable. Local ambient temperature was sensed via a resistance thermal device (RTD) sensor mounted in a shaded area outside of the HIVAS flowfield. Using previously obtained flow survey data and the local ambient pressure and temperature measurements, the sensed pressure from the riser pitot tube was corrected to give dynamic pressure at the chute skirt. Mach number and flow velocity at the chute skirt were also computed and displayed in real time. Figure 12 shows the parachute mounted to the test fixture in HIVAS ready for testing. The pitot probe on the riser line is also shown in Fig. 12.

During phase-II, several variations of the elastomer hoop and attachment, such as routing the 0.5-in.-cross-sectional-diam hoop through a Teflon® sleeve that was in turn run through Teflon-covered keeper loops sewn to the radials, were tested. The two surviving designs (24% ribbon and ring-slot parachutes) from phase-I were retested, along with a lighter-weight 9-ft-diam ribbon parachute supplied by personnel from NASA Johnson Space Center (JSC). This chute had been previously used as the pilot chute for the space shuttle landing/deceleration system. The shuttle pilot chute had well-known aerodynamic characteristics and provided a good control to verify that the elastic reefing system was not detrimentally affecting the chute inflation properties.

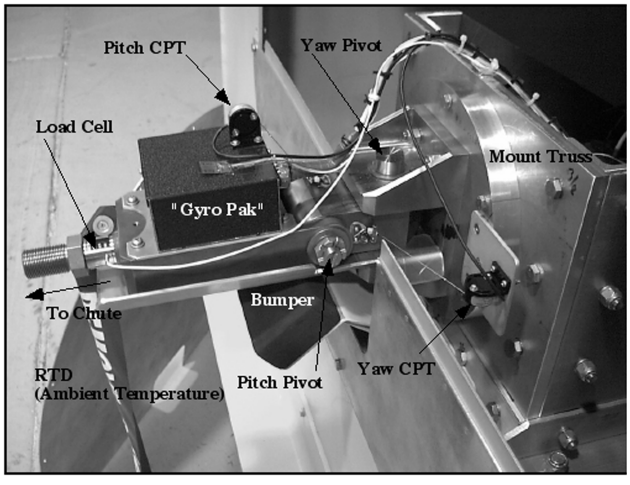

Fig. 11 Parachute-load force balance.

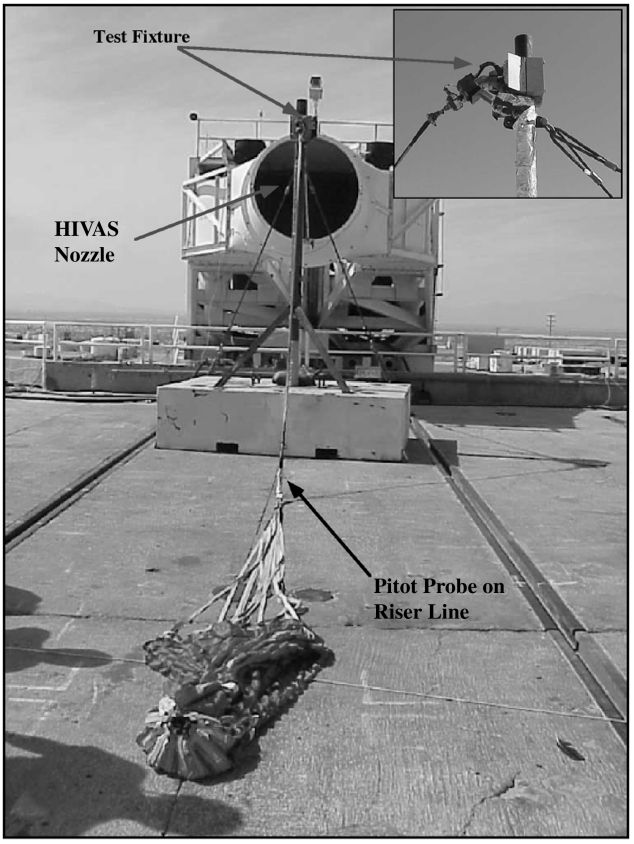

Fig. 12 Parachute installed at HIVAS and ready for testing.

Again during phase-II testing, the performances of the 24% ribbon and ring-slot parachutes were unacceptable. The 24%-porosity ribbon parachute exhibited a propensity to inflate, spill air, deflate, and then reinflate in a matter similar to the movements of a jellyfish or squid. The ring-slot design would fully inflate, but had high-amplitude coning instabilities that exceeded the X-37 requirements. A 1.0-in. slot in the upper canopy near the vent of the ring-slot parachute was added in an attempt to increase the coning stability, and the modified chute was hard-line reefed to 73% of the nominal opening diameter. These modifications improved the stability, but the design still did not meet the X-37 coning-angle requirements.

When the space shuttle pilot chute was tested as an evaluation of the elastomer reefing system and HIVAS flow effects, the chute inflated well and was extremely stable. As a final test during this phase, a 0.25-in.-cross-sectional-diam elastomer line inside a Teflon sleeve with a spectra overinflation control line was attached to the shuttle pilot chute using Teflon-covered keepers. This test was performed to determine if the collapse mechanism detrimentally effected the chute performance. The system worked quite well and did not affect the inflated drag area or stability characteristics. As the flow velocity was ramped down at the end of the test run, the elastomer line worked as designed, reducing the drag area by about 50%, and allowed the JSC pilot chute to drop from the flowfield earlier than the chute without the reefing package.

The conclusion of the phase-II testing was that the original parachute designs were inadequate. The large differences between the performance of the lightweight space shuttle pilot chute and the heavier 24% ribbon and ring-slot parachutes indicated a need to revise the original parachute designs. Although it is likely that the airflow pattern of the HIVAS system contributed to the inflation and stability problems with the original designs, the heavy chute weights and excessive porosities were a more likely cause of the problems. For example, the fact that the 24%-porosity ribbon parachute inflated well at lower speeds (drop tests) but would not open at higher speeds was indicative of excessive geometric porosity. The stability problems of the ring-slot parachute were likely a result of excessive slot length, too large of a canopy weight for a given size, or a combination of both. The elastomer reefing system did not appear to be a contributing factor to these performance flaws. In any case, it was clear that the original designs were flawed and a new design was necessary to meet the X-37 requirements. The redesign necessitated a third phase of high-speed testing at the HIVAS facility. Figure 13 shows a visual comparison of the three parachutes inflated in the HIVAS flowfield.

C. HIVAS Phase III

Following the end of phase-II, a new set of parachutes was developed for phase-III testing. The instrumentation system was identical for the phase-III testing, except that the original load cell, a lightweight microelectronic mechanical system design, was replaced by a heavier, more robust, load cell. It was feared that the original load cell would not survive the cumulative 90 min of endurance testing at full flight dynamic pressure. Small adaptations to the force balance were required to accommodate the heavier load cell. The parachute designs tested during HIVAS phase-III were modified to overcome the shortcomings discovered during the phase-I and phase-II tests. For the phase-III HIVAS, a total of eight parachute designs were tested. These designs include 1) two JSC-supplied shuttle pilot chutes, reefed for different drag areas to assess the effect on stability, 2) two enhanced-durability JSC pilot chute "clones" designed and fabricated by NAWC, 3) and four revised ribbon chute designs fabricated by the original subcontractor. Phase-II test results indicated that the JSC shuttle pilot chute design appears to have correct porosity (19.8%), allowing for proper inflation and stability across a range of dynamic pressures. The NAWC designs reproduced the characteristics of the JSC pilot chute closely, with only the strength of the horizontal ribbon material being modified. The other four designs differed more significantly from JSC pilot chute design and offered a wider variation in layout geometries. The parameter sets corresponding to the parachute design tested during phase-III are listed in Table 2.

As with the earlier test phases, the objectives of the phase-III tests was to down-select to the two best designs to carry forward to flight. In the initial part of the phase-III tests, each of the chutes was tested briefly (2–4 min) at flight dynamic pressure. Because a much wider array of chutes were tested, a more objective criterion was needed to select the best chutes. An analytical metric was developed to allow the relative merits of the chute designs to be compared. The metric incorporated the criteria listed in earlier into a single performance index J, where a smaller value indicates better performance. The metric decided on by the ALTV test team is

$$J = A \times \left\| \frac{C_D A_{\text{mean}} - 29.15\ \text{ft}^2}{29.15\ \text{ft}^2} \right\| + B \times \sqrt{\frac{1}{N}\left(\sum_{i=1}^{N} \left[\theta_i^2\right] + \sum_{i=1}^{N} \left[\psi_i^2\right] \right)} + C \times \frac{\sqrt{\frac{1}{N}\sum_{i=1}^{N} [C_D A_i - C_D A_{\text{mean}}]^2}}{C_D A_{\text{mean}}} + D \tag{9}$$

The first term on the right-hand side of Eq. (9) penalizes a design for which the drag area deviates from the desired drag area. The second term penalizes for coning oscillation and is a measure of coning stability. The third term penalizes for variations in the instantaneous drag area and is an indication of inflation stability. The final term was a subjective bias and was reserved as a tiebreaker when two chutes had otherwise identical performance. For example, if two chutes have the same value for J based on the first three criteria, then the chute constructed of the least expensive or strongest material wins. The weights $\{A, B, C, D\}$ were chosen to balance the relative magnitudes and importance of the terms. For these tests, the values used were $\{1.0, 2.0, 2.0, 1.0\}$.

Based on the index analysis discussed already, the parachutes selected for endurance testing were a NAWC design (NAWC 1) identical to the JSC design but with slightly stronger ribbons and a modification of the original 24% ribbon design (MOD 3) that exhibited very good coning and inflation stability. The measured drag areas were 29.05 ± 1.45 and 30.15 ± 1.78 ft^2, respectively.

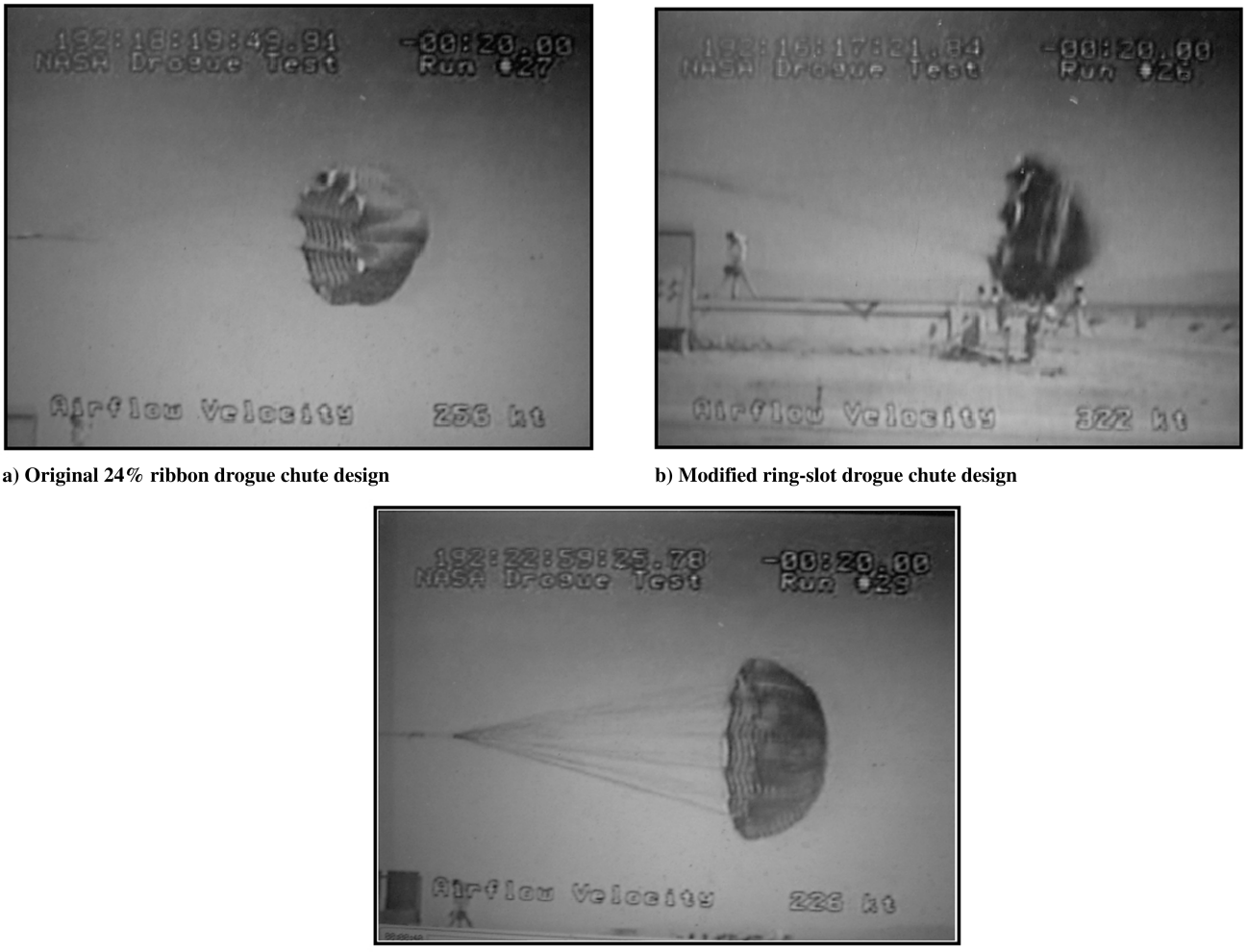

a) Original 24% ribbon drogue chute design

b) Modified ring-slot drogue chute design

c) JSC/space shuttle pilot chute design

Fig. 13 Visual comparison of inflation characteristics of HIVAS phase-II chute designs.

The drag areas of the parachute were calculated by dividing the sensed axial load on the force balance by the corrected (adjusted for HIVAS flow effects) impact pressure sensed by the riser pitot probe. The mean drag area and corresponding standard deviation were calculated using steady-state inflation data selected by visual inspection from each of test run.

These two parachutes were fitted with the improved elastomer hoops and subjected to 45 min of flow exposure at the flight dynamic pressure. The improvements made to the elastomer hoops included forming them as 0.25-in.-cross-sectional-diam solid bands without a joint, encasing three of them in a Teflon sleeve, and attaching a spectra line in the sleeve seam to act as an overinflation control line. The bands were then routed through Teflon-covered Kevlar keeper loops sewn to the radial joint at the skirt. The three smaller cross-sectional lines provided sufficient tensile force to reef the parachute, but also provided some measure of redundancy in case one of the lines failed. The external view of the modified reefing system is shown in Fig. 14.

During the endurance tests, the parachutes were subjected to 15 min of continuous flight dynamic pressure and then the engines shut down to allow a visual check for damage before the next 15-min test. To evaluate the elastomer system, the HIVAS airspeed was ramped down slowly each time, to visually monitor the parachute skirt collapse, as well as to log the drag data for evaluation. The NAWC-1 chute was tested first, and at the end of the first 15 min, there was no parachute damage, but one of the three-elastomer hoops had broken. After the next 15 min, there was some wearing damage evident on some of the Teflon keeper loops and the Teflon covering the vent tapes, and the second elastomer hoop had broken. During the final 15-min run, the final elastomer hoop broke, but there was no additional damage to the parachute. After the test, inspection of the elastomer system indicated that the individual bands (because they

Table 2 Parameter matrix for chutes tested during HIVAS phase-III

Chute name	Nominal diameter, ft	Type	Canopy angle, deg	Geometric porosity, %	Design C_DA, ft^2	Horizontal ribbon strength, lb
JSC 1	9.0	Ribbon	20	19.8	28.50	300
JSC 1	9.0	Ribbon	20	19.8	28.50	300
NAWC 1	9.0	Ribbon	20	19.8	29.17	460
NAWC 2	9.0	Ribbon	20	19.8	29.17	550
MOD 1	9.5	Ribbon	20	19.8	29.17	300
MOD 2	9.5	Ribbon	20	22.0	29.17	460
MOD 3	9.5	Ribbon	20	24.0	29.17	460
MOD 4	8.5	Ribbon	20	24.0	28.50	1000

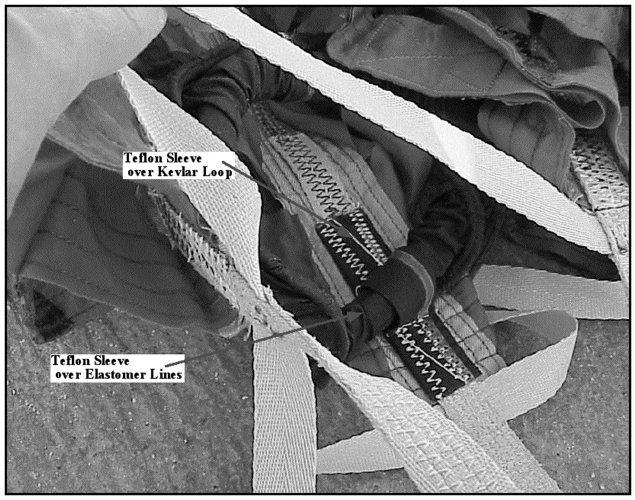

Fig. 14 Attachment of modified elastomer reefing package to skirt.

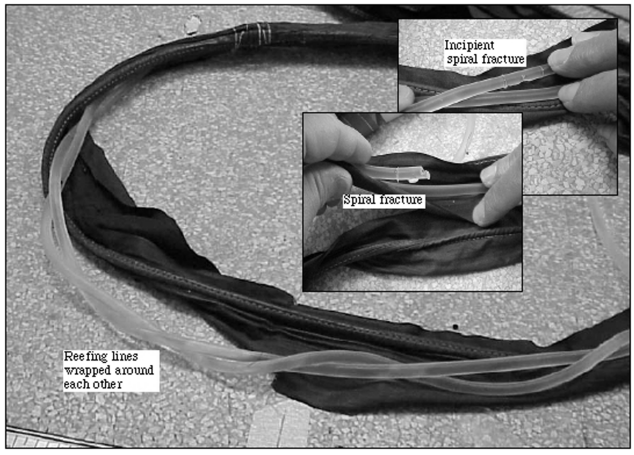

Fig. 15 Posttest inspection of elastomer reefing system failure.

were all together in a single sleeve) became entangled, causing a single segment to stretch farther than 100% (a likely cause of the line breakage). Figure 15, taken at the postflight inspection, shows the elastomer lines entangled within the Teflon sleeve.

To compensate for the failure mode shown in Fig. 15, the elastomer system on the MOD-3 design was altered so that there were two bands, each in is own Teflon sleeve, inside a larger Teflon sleeve. It was felt that by reducing the binding friction on the bands, the propensity to wind around each other would diminish. Two bands were used instead of three, because they would not fit into the available outer sleeve and the keeper lops that attached the package to the chute. The MOD-3 chute was tested for the first 15 min. Visual inspection indicated that there was minimal parachute damage, and both elastomer bands were intact. After the next 15 min, a small amount of wear on the Teflon of the keepers was noted, and one of the elastomer bands had broken. Midway into the last 15 min of testing, the second elastomer broke (drag data jumped somewhat), but the parachute damage again was minimal at the conclusion of the 45 min. Upon inspection of the elastomer system, it appeared that the inner Teflon sleeve hems had unraveled and tangled together, again causing uneven loading on the bands, resulting in their rupture. The unraveling was a result of the quick-fix sewing techniques used to construct these sleeves.

As a final check on the functionality of the elastomer reefing system, a test was performed with the remaining JSC parachute that had an intact dual-line elastomer system installed. This package was identical to the MOD-3 system. For this test, the JSC chute was tested for about 15 min at flight dynamic pressure, and then the air speed was ramped up and down at the end of the 15-min interval. When all the drag data from tests with and without the elastomer system were put together, it was very obvious that the elastomer system was working. These data are presented in Figs. 16 and 17. Figure 16 plots the computed drag area versus dynamic pressure for nine inflation/deflation cycles obtained *without* the elastomer present. As soon as the chute inflates, the C_DA "cloud" remains relatively constant, hovering between approximately 25 and 33 ft^2. The data presented in Fig. 16 are typical of those used to calculate the mean parachute drag area and standard deviation.

Figure 17 plots the computed drag versus dynamic pressure for nine inflation/deflation cycles obtained *with* the elastomer reefing system present. In this case, there are two C_DA clouds: one hovering at 25 to 30 ft^2 and the other hovering much lower, between 1 and 10 ft^2. The dropoff from the upper cloud to the lower cloud depends on the number of surviving elastomer bands still present in the reefing system and on whether the chute is inflating or deflating. Clearly, more drag force is required to inflate the chute than to deflate it, and so there is hysteresis in the up and down curves. The important point to take away from Fig. 17 is that the elastomer system reduces the drag area significantly at low dynamic pressures. The 9-run statistical average of the reefed drag area, when the reefing system had collapsed the chute skirt, was approximately 42.0 + 15.6% of the unreefed drag area of the chute.

Also note that the inflation cycle tends to follow a nonlinear path. For a typical ribbon parachute, the drag area typically increases

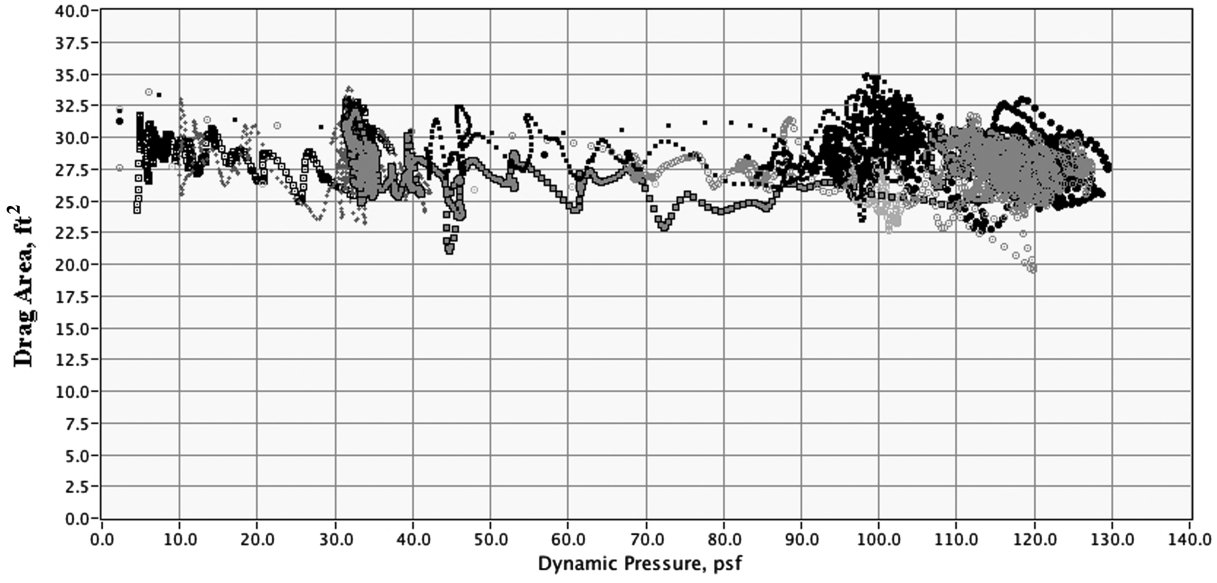

Fig. 16 JSC pilot chute, variation of C_DA with dynamic pressure, no elastomer reefing system attached.

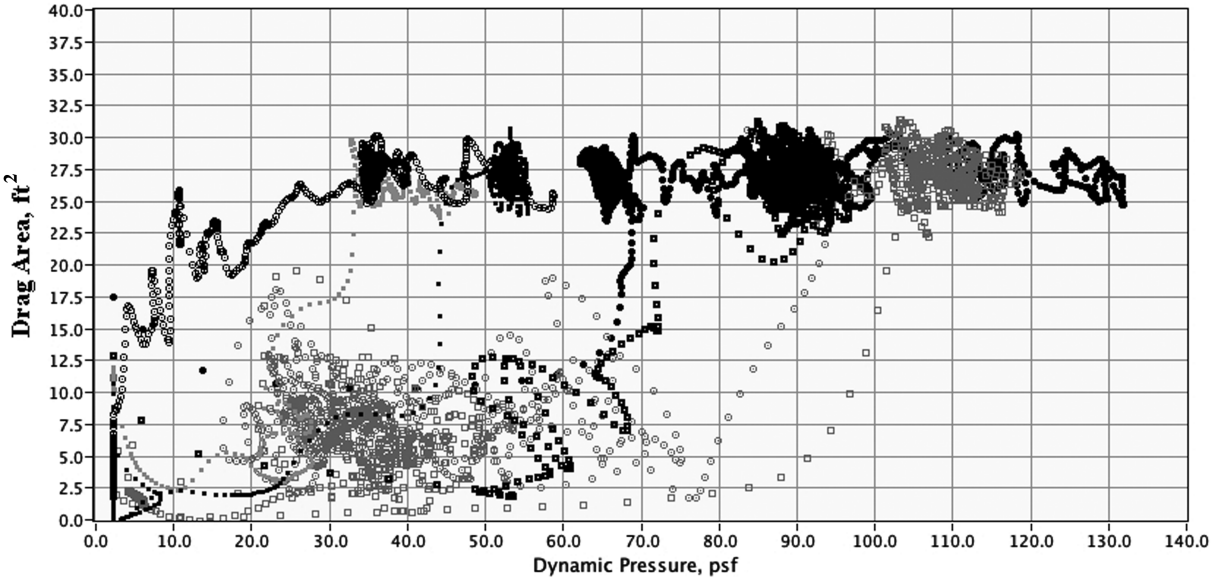

Fig. 17 JSC pilot chute, variation of C_DA with dynamic pressure, with elastomer reefing system attached.

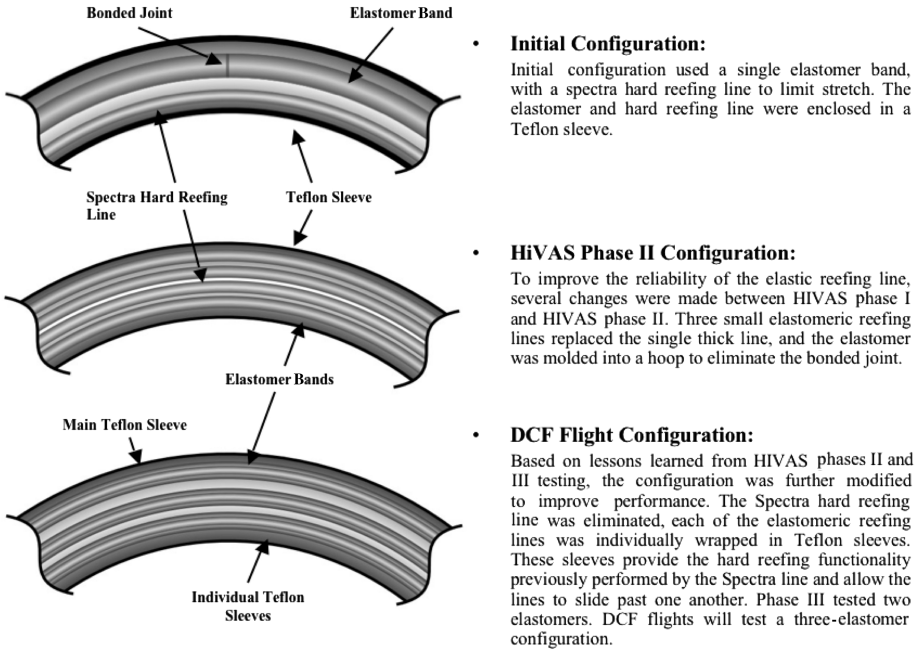

Fig. 18 Evolution of the elastomer reefing package during HIVAS tests (DCF indicates the drogue chute fixture).

almost linearly with time [8] during the inflation cycle. The elastomer reefing system has the effect of delaying the opening time significantly when compared with an unreefed parachute. The initial drag are will increase almost linearly with time until the elastic band comes into tension, then the rate of increase of the drag area will "roll off," with time increasing ever more slowly as the elastomer is stretched. For a free-flying deployment, this inflation delay has the effect of significantly reducing the opening shock load of the parachute. When properly sized, a similar passive-reefing system could eliminate the need for staged reefing and line cutters and offer a significant reduction to the complexity of the decelerator system. This topic is promising area for future research.

Even though the two-band elastomer system did not survive the entire endurance testing, it did show improved durability. The testing window at HIVAS closed before further design changes could be made with regard to the elastomer system. It is believed that if a third band had been installed, the system would have survived with full functionality for the duration of the endurance testing. In preparation for the follow-up flight tests, the elastomer system was again modified, this time sewing three bands into a three-leaf-clover-style outer sleeve, such that each band is separated from the others and there are no inner seams to ravel and become tangled. Figure 18 shows the evolution of the reefing system throughout the HIVAS tests and the final configuration that was brought forward for flight-testing.

Because the NAWC-1 and MOD-3 parachutes had successfully met the test criteria, they were both selected for the B-52 flight-testing. Unfortunately, the drogue chute portion of the ALTV program was canceled before the B-52 flights. As mentioned in the Introduction, the X-37 was successfully dropped from the Scaled Composites White Knight carrier aircraft in April 2006 and completed testing during 2006.

VII. Conclusions

A collapsible drogue parachute system developed for the X-37 approach and landing test vehicle (ALTV) is described. The high altitude at drogue release allowed predominant winds to take the chute off the Edwards Air Force Base test range and into the flight corridors of major commercial airports. A mechanism to collapse or

significantly reduce the drag area of the drogue was required to keep the landing point within the test range after the parachute was jettisoned from the test vehicle. A simple passive mechanism that relied on a silicone band attached at the drogue skirt was developed. The design for this drag reduction system is similar to a conventional parachute reefing system. In this approach, however, an elastic line replaces the traditional reefing hard line. When the chute is deployed under full drag load, the elastic line is stretched out and does not significantly affect the drag. When the load is reduced, the elastic contracts to alter the drogue chute shape, reducing the drag. This report details the results of the development and testing on this reefing system. Details and reasons for the design evolutions are described. At low dynamic pressures, the final design that emerged from both low-speed and high-speed ground testing was demonstrated to reduce the drag area to approximately 42% of the unreefed drag area. Based on the testing performed on this reverse reefing system, using an elastomer band appears to be a satisfactory method of reducing the drag of a parachute after its jettison from a payload. When properly sized, a similar passive-reefing system could eliminate the need for staged reefing and line cutters and offer a significant reduction the complexity of the decelerator system. This topic is a promising area for future research.

References

[1] Whitmore, S. A., Cobleigh, B. R., Jacobson, S. R., Jensen, S. C., and Hennings, E. J., "Development and Testing of a Drogue Parachute System for X-37 ALTV/B-52H Separation," NASA TM-2004-212044, Jan. 2004; also AIAA Paper 2004–873, Jan. 2004.

[2] David, L., "X-37 Flies at Mojave But Encounters Landing Problems," *Space.com*, 7 Apr. 2006, http://www.space.com/missionlaunches/060407_x37_drop.html [retrieved 06 July 2007].

[3] David, L., "U.S. Air Force Pushes for Orbital Test Vehicle," *Space.com*, 16 Nov. 2006, http://www.space.com/news/061117_x27b_otv.html [retrieved 06 July 2007].

[4] *Range Reference Atmosphere Climatology* [online database], https://bsx.edwards.af.mil/weather/rcc.htm [retrieved 31 Aug. 2006].

[5] Wolf, D. F., and Croll, R. H., "Wind-Tunnel Measurements of Dynamic Reefing Line Force in Ribbon Parachutes," *Journal of Aircraft*, Vol. 18, No. 1, Jan. 1981, pp. 30–34; also AIAA Paper 79-0465R, May 1979.

[6] "U.S. Standard Atmosphere, 1976," National Oceanographic and Atmospheric Administration, NASA, and U.S. Air Force Special Report, 1976, pp. 10–15.

[7] Knacke, T. W., *Parachute Recovery Systems Design Manual*, Para Publishing, Santa Barbara, CA, 1992, Chaps. 5, 6.

[8] Whitmore, S. A., Fife, M. J., and Brashear, L. A., "Development of a Closed-loop Strap Down Attitude System for a High Altitude Flight Experiment," AIAA Paper 97- 0537, Jan. 1997.